Landsliding triggered by reservoir operation: a general conceptual model with a case study at Three Gorges Reservoir

Jinge Wang, Wei Xiang & Ning Lu

Acta Geotechnica

ISSN 1861-1125

Acta Geotech.
DOI 10.1007/s11440-014-0315-2

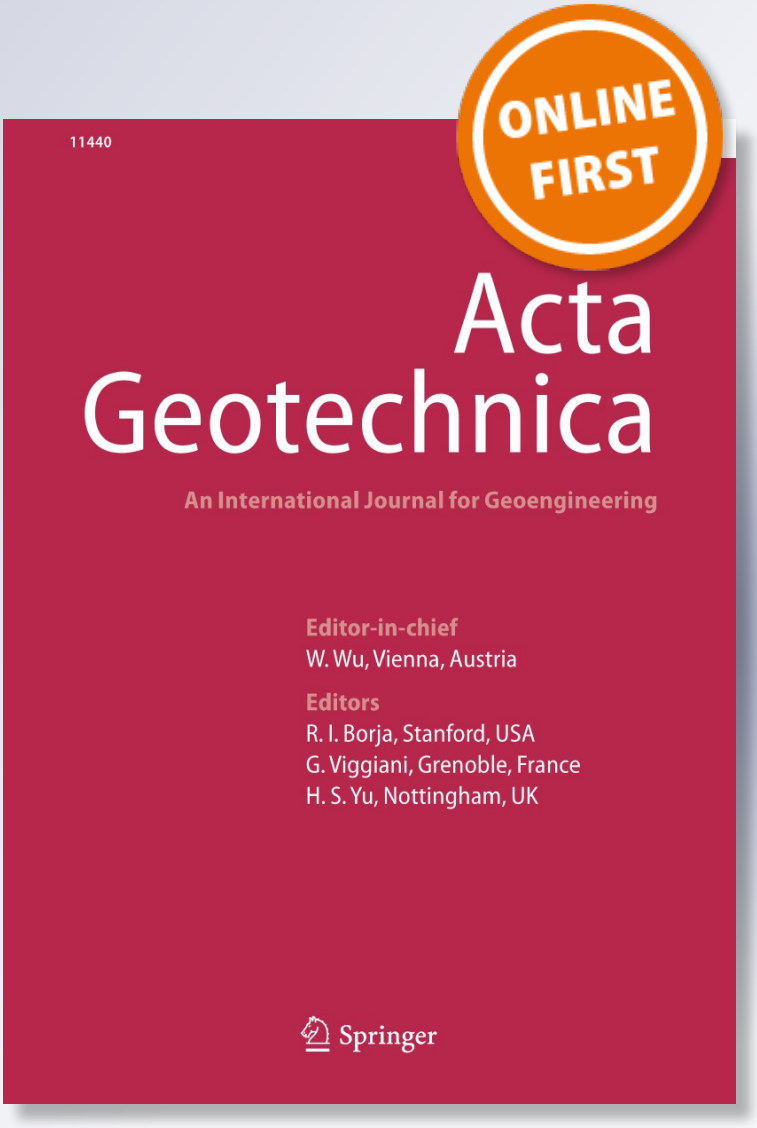

Springer

Acta Geotechnica
DOI 10.1007/s11440-014-0315-2

RESEARCH PAPER

Landsliding triggered by reservoir operation: a general conceptual model with a case study at Three Gorges Reservoir

Jinge Wang · Wei Xiang · Ning Lu

Received: 7 January 2013 / Accepted: 20 March 2014

Abstract The Three Gorge Reservoir, one of the largest civil engineering projects in human history, dams the Yangtze River to form a 660-km-long and 1.13-km-wide reservoir. Today, although the project has been completed and is in normal operation, the on-going landslide initiation and movement in response to the reservoir operating is one of the main geologic hazards. The Huangtupo (meaning "yellow soil slope" in Chinese) Slope typifies such on-going landslides along the reservoir. Observations from a multi-year monitoring program conducted on this slope indicate that there are multiple slides on the reservoir banks that move episodically into the reservoir and their movements appear to be highly correlated with the initial and seasonal changes in the reservoir pool level. A hydro-mechanical numerical model is constructed to investigate the quantitative links among the episodic movements and the variations in pore water pressure, suction stress, hydrostatic reservoir water loading, and slope self-weight induced by the fluctuating water levels. Modeling results identify regions within the variably saturated slope where significant changes in stress occur during the periods of the initial impoundment that raised water levels from 68 to 135 m and that occur in response to seasonal fluctuations of the reservoir pool level between 145 and 175 m. We find that the rise or decline of reservoir pool level can either increase or decrease the stability of landslide. In general, hydrostatic reservoir water loading has positive correlation with the stability; pore water pressure and suction stress have negative correlation with the stability; and the effects of slope self-weight depend on the dip angle and mechanical properties of sliding surface.

Keywords Effective stress · Factor of safety · Landslide · Reservoir operation · Slope stability · Unsaturated soils

1 Introduction

The Three Gorges Water Conservancy and Hydropower Project is the largest hydropower project in the world and one of the largest civil engineering projects in human history. The reservoir is located on the main stem of the Yangtze River between Yichang (city) and Chongqing (city) in China with a length of 660 km and an average width of 1.12 km (Fig. 1). The project was completed in 2008 and began normal operation at that time. Due to the complex geological settings and subtropical climate, the lakeshore along the 660-km-long reservoir presents many geologic and environmental hazards to the residents of the area such as landslides [11], increased sedimentation [23], water pollution [29], reservoir-induced seismicity [13], and the potential for landslide-induced seiche [25]. These geologic hazards are in part a manifestation of the disturbance of the original environment created by this civil work.

Reservoir-induced landslides present a challenge to society that seeks to benefit from the hydroelectric power and flood control that large reservoirs can provide. According to recent study, there exist more than 2,000

J. Wang (✉) · W. Xiang
Three Gorges Research Center for Geo-hazard,
China University of Geosciences, Wuhan 430074, China
e-mail: wangjinge1985@gmail.com

W. Xiang
e-mail: xiangwei@cug.edu.cn

N. Lu
Department of Civil and Environmental Engineering,
Colorado School of Mines, Golden, CO 80401, USA
e-mail: ninglu@mines.edu

Published online: 13 May 2014

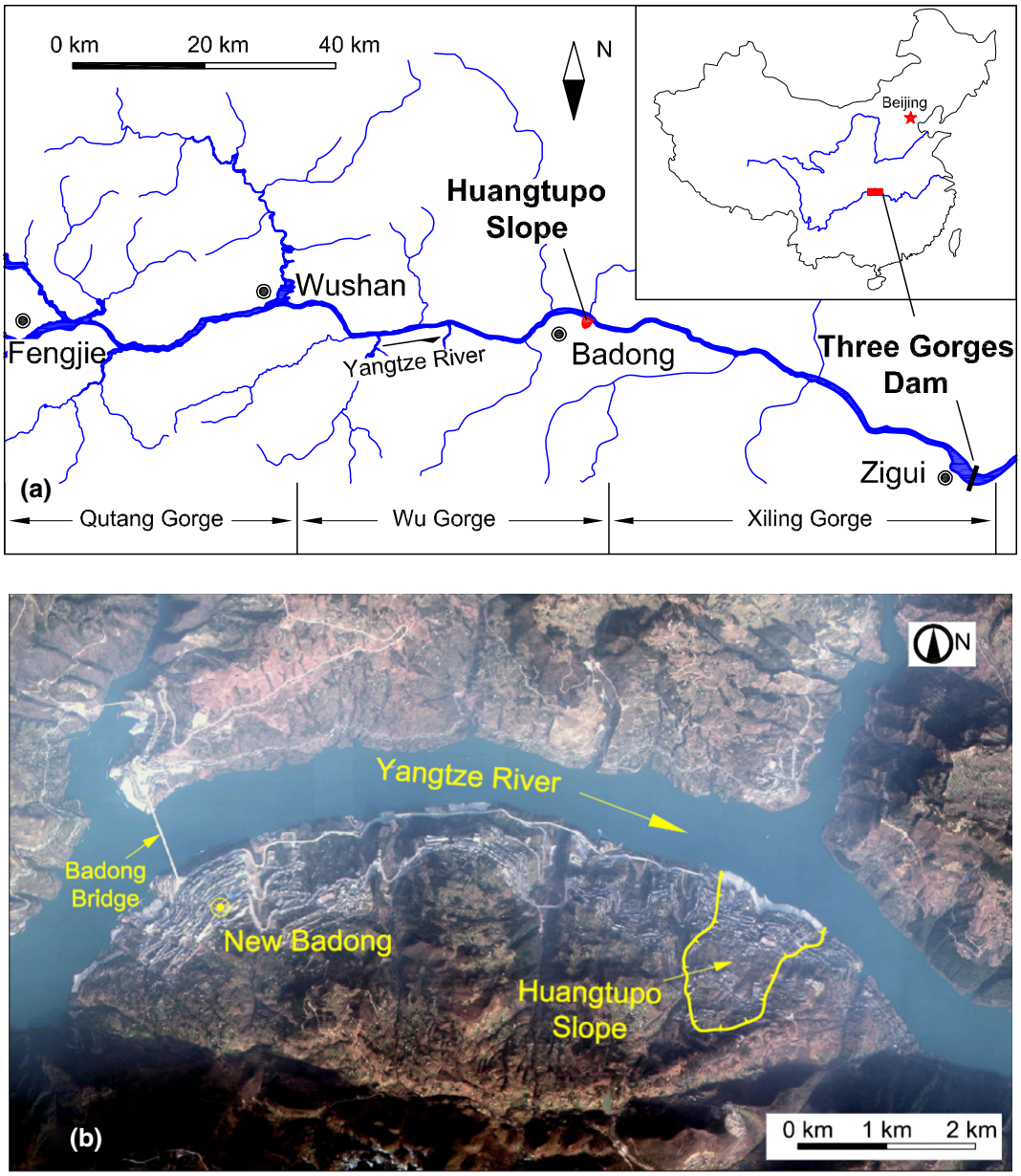

Fig. 1 Location of the Huangtupo Slope with respect to: **a** the Three Gorges and **b** Badong county

landslides of different sizes in the Three Gorges Reservoir area [12]. And among them, at least 250 are identified as large-scale landslides with volumes greater than 10^6 m^3 [26]. One of the main triggering mechanisms for these landslides is believed to be the initial reservoir impoundment and consequent annual water-level fluctuations.

Reservoir-induced landslides are quite common in many parts of the world. According to the investigation in the Grand Coulee Reservoir area along Columbia River, during the period of 1941–1953 [10] about 49 % of the landslides occurred during the initial impoundment period and about 30 % occurred with the annual decrease in water level. In Japan, about 60 % of the reservoir-induced landslides occur during reservoir drawdown and about 40 % occur when water levels rise [8]. Thus, landslides can be induced by both water-level rise and decline, and by both initial reservoir impoundment and the annual water-level fluctuations associated with reservoir operation, depending on geologic and hydrologic conditions.

Many researchers have studied the landslide problems in Three Gorges Reservoir area since the beginning of this huge water conservancy and hydropower project. Researchers with geological background generously study these problems on the base of geological analysis (e.g., [4]), and some other researchers evaluate the stability of the landslides through the surface or deep deformation

monitoring data (e.g., [18]). However, for the periodical water-level variation in the reservoir, certain parts of wading landslides are under the drying and wetting circulating condition. So, the stability of reservoir wading landslides not only depends on their geological conditions and other common landslides triggering factors such as rainfall and earthquake, but also influenced by the hydro-mechanical properties of sliding mass and the variation in water level significantly. This paper intends to study this problem by employing basic theories of unified saturated–unsaturated soil mechanics framework.

2 Huangtupo Slope and site geology

The Huangtupo Slope is located in Badong County on the south bank of the Yangtze River between Wu Gorge and Xiling Gorge in the Three Gorges Reservoir area (Fig. 1a, b). Qutang Gorge, Wu Gorge, and Xiling Gorge are the Three Gorges and stretch 120 km behind the Three Gorge Dam (Fig. 1a). As part of the Three Gorges Water Conservancy and Hydropower Project, a portion of the population in Badong County that originally resided below 175 m elevation was moved to the Huangtupo Slope starting in 1984. However, in recent years, the Huangtupo Slope was found to be an old dormant landslide. The main evidence indicating that the slope is a landslide are two obvious movement events that occurred in 1995 prior to the initial reservoir impoundment [4]. Monitoring data from 2003 to 2008 indicates that the cumulative displacements in the toe region of Huangtupo Slope are 80–148 mm, and the maximum displacement rate reaches 12.08 mm/month. Because more than 10,000 people currently reside on the Huangtupo Slope, and the slope is located on the waterway of the Yangtze River, its stability is of great public concern. Several researchers have previously studied the formation mechanism and stability of the Huangtupo Slope. On the basis of field mapping and electrical resistivity surveys, Deng et al. [4] investigated the structural and deformation history of the Huangtupo Slope and developed a three-stage model that involves sequential processes of mass rock creep, primary landsliding, and partial reactivation of the landslide. Wen et al. [27] and Wen and Chen [26] focused on the composition and mechanical properties of the slip zones in the Huangtupo Slope. Liu et al. [18] employed an advanced InSAR time series technique to monitor the movements of earth surface of Huangtupo Slope. Based on both the InSAR and the GPS monitoring data, qualitative correlation between annual landslide movements and water-level changes has been suggested [18].

While a new wave of population migration from the Huangtupo Slope to the New Badong County (Fig. 1b) is under way, further scientific investigations are being conducted. For example, the Three Gorges Research Center for Geo-hazards has constructed a 1.1-km tunnel in the bedrock beneath the No. 1 slide at Huangtupo Slope for in situ monitoring and testing, together with surface and subsurface monitoring and modeling on and within the Huangtupo Slope (Fig. 2). This research is part of this systematic investigation program.

The landform of the Huangtupo area is a polygonal-shaped slope that dips toward the river with the highest ground at the south bound and the lowest at the north bound (Fig. 2a). The slope is inclined at the upper, middle, and bottom parts at about 30°, 18°, and 33°, respectively (Fig. 2b). Generally, the Huangtupo landslide surfaces are almost of the same dip direction of the underlying bedrock that is limestone or pelitic limestone except the toe area. Due to the past landslide movement, several gently sloping platforms have formed on the surface of the sliding mass (Fig. 2b). Ravines have also developed on the sloping surface. Due to the geologic control of Badong fracture–fault system, the ravines run mainly north–south and are distributed along the major joints and fractures (Fig. 2a). The Huangtupo Slope has been cut into several parts by the ravines, which form several separate landslide bodies. Bedrocks below the sliding mass are visible in some locations at the bottoms of some deep ravines.

According to the site geologic survey [9], the Huangtupo Slope can be divided into 4 separate landslide bodies (Fig. 2a), namely the No. 1 slide, which is adjacent to the reservoir in the northwest; the No. 2 slide, which is also adjacent to the reservoir in the northeast; the No. 3 slide, which is locally called the "Garden Spot Landslide" in the southwest; and the No. 4 slide, which is locally called the "Transformer Station Landslide" in the southeast (Fig. 2a). The Huangtupo Slope consists mainly of loose to dense soil and rock debris as thick as 90 m. The volume of the total 4 sliding bodies is $\sim 6.9 \times 10^7$ m^3. Because the No. 1 and No. 2 slides are adjacent to the reservoir, their stabilities are likely affected by the fluctuation of the water level in the reservoir. Investigation report [9] indicates that Huangtupo slope is a large and complex landslide with multiple sliding times and slides. Controlled by the shapes of topography and cutting of deep ravines, the movements of the four slides of the Huangtupo Slope are generally independent. However, because the toes of the No. 3 and the No. 4 slides overlap considerably with the crests of the No. 1 and the No. 2 slides, motion of the No. 1 and the No. 2 slides likely influences movement of the No. 3 and the No. 4 slides.

This study focuses on the No. 1 slide. Field investigation indicates that the No. 1 slide has a length of 770 m from

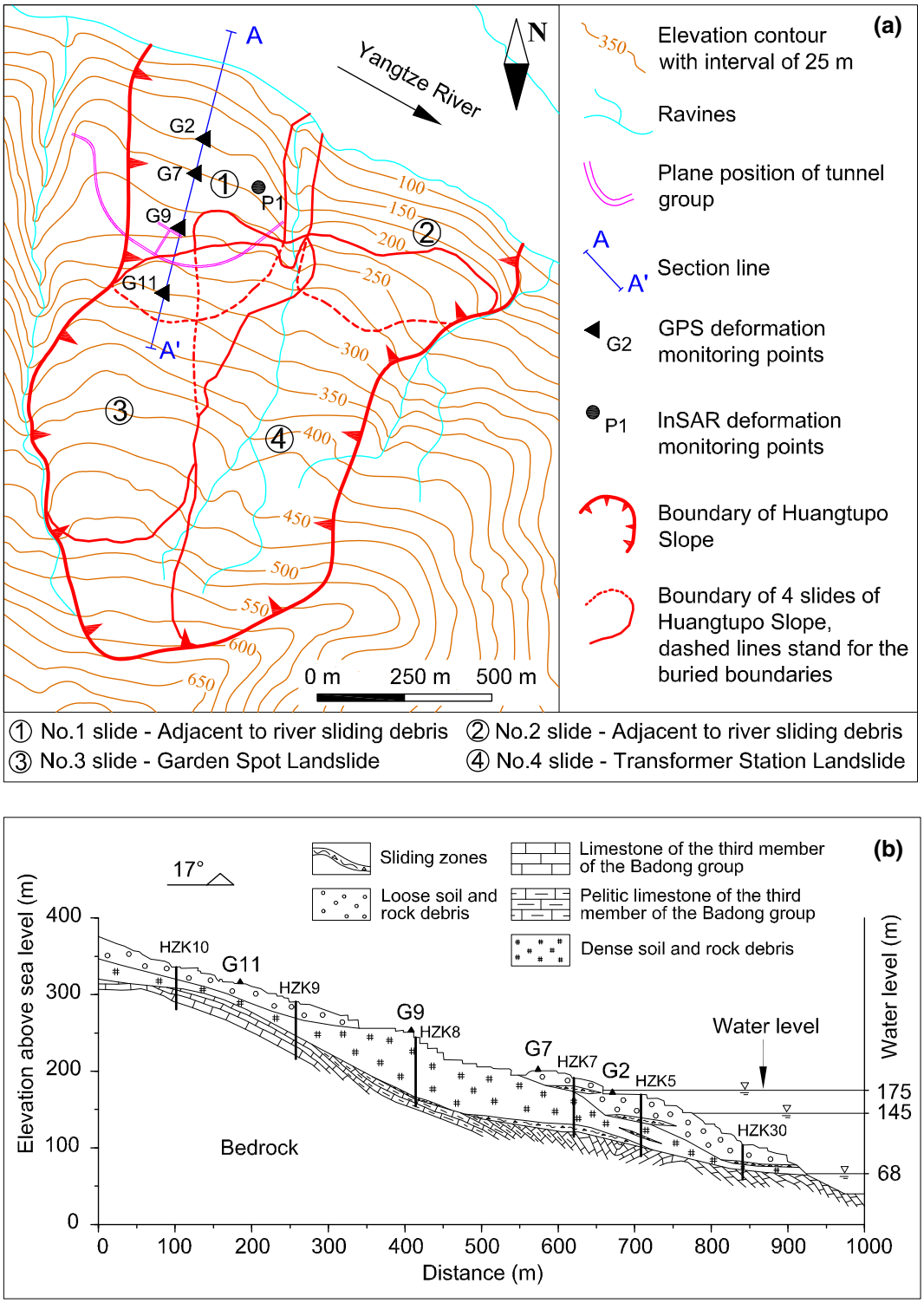

Fig. 2 Site geologic conditions and investigation at the Huangtupo Slope: **a** a plan view map showing four separate landslides; the northwest slide or the No. 1 slide, the northeast slide or the No. 2 slide, the southwest slide or the No. 3 slide (locally called the "Garden Spot Landslide"), and the southeast slide or the No. 4 slide (locally called the "Transformer Station Landlside"), and **b** cross section along A–A′ through the No. 1 slide

north to south and a width of 480 m from east to west (Fig. 2a). The area and volume of this slide are about 3.25×10^5 m^2 and 2.26×10^7 m^3, respectively. From the field mapping and borehole drilling shown in Fig. 2b, the bedrock of No. 1 slide is limestone and pelitic limestone of the third member of the Badong group (T_2b^3) [9]. The

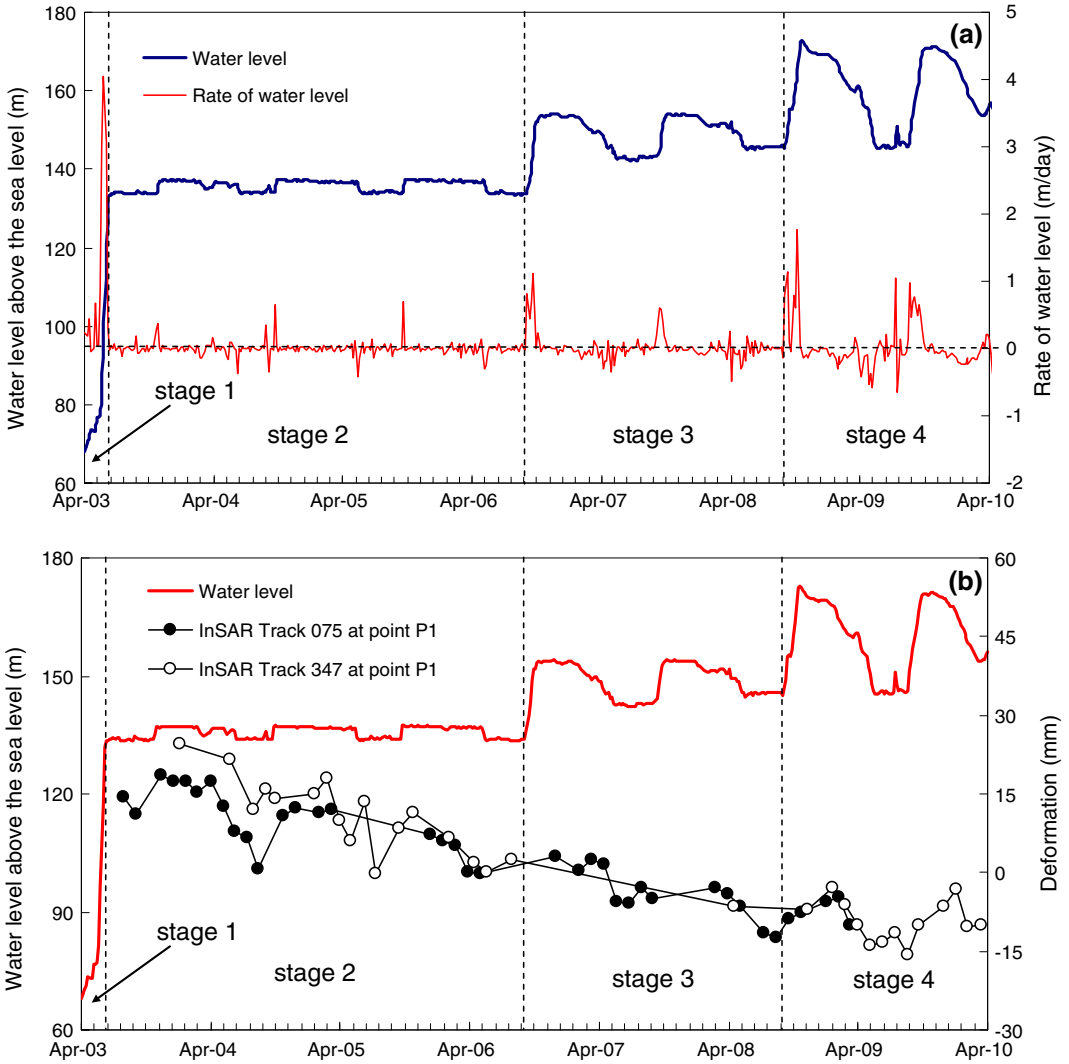

Fig. 3 Records of: **a** the reservoir water-level variation in the Three Gorges Reservoir from April 2003 to April 2010 (in meters above sea level), and **b** time series deformation for P1 in the radar line of sight direction derived from InSAR Tracks 075 and Tracks 347 where negative values mean that the ground surface moves away from the satellite and likely indicate landslide movement (data from [18])

materials of No. 1 slide are either *loose soil and rock debris* originated from gray pelitic limestone or *dense soil and rock debris* originated from gray limestone (Fig. 2b). Borehole data indicate that there are two major sliding zones developed within the No. 1 slide (Fig. 2b). The main sliding zone is located between sliding mass and bedrock and between boreholes HZK5 and HZK8 (Fig. 2b), and the other is located within the sliding mass between the dense soil and rock debris and the loose soil and rock debris and is centered on borehole HZK5 (Fig. 2b). The sliding zone soils are celandine green silty clay with 5–20 % gravel. Because the strength and permeability of sliding zones are both the lowest in the landslide body (see Table 2), these sliding zones not only can control the stability of the landslide, but also influence the local movement of groundwater and pore water distribution.

3 Mechanisms for reservoir-induced landslides

Like many other landslides in the Three Gorges Reservoir area, the No. 1 slide at the Huangtupo Slope is a wading landslide, which means that the elevation of the toe is below the water level of the reservoir. Beginning with the impoundment of Three Gorges Reservoir, the variation in water level in front of Huangtupo Slope has experienced 4 stages, as shown in Fig. 3. The first stage is from April 2003 to June 2003 when the water level was raised from 68 to 135 m in less than 3 months. The second stage is from July 2003 to September 2006, when the water level was maintained at about 135 m. The third stage is the initial fluctuation period from the end of September 2006 to September 2008 when the water level varied annually between 145 and 153 m. The fourth stage is characteristic

of the normal operation of the reservoir after the end of September of 2008 when the water level fluctuates annually between 145 and 175 m.

The impacts of the initial impoundment and annual water-level fluctuations on the stability of slopes adjacent to the reservoir can be quantitatively assessed by analyzing the roles of changes in hydrostatic water loading on the slope, pore water pressure below the water table, suction stress above the water table, and slope's self-weight in terms of factor of safety of the slope. The factor of safety (FS) for a given failure surface can be used to synthesize all these previously mentioned mechanisms and be defined as either the ratio of shear strength (resistance) along the failure surface to the driving shear force or the ratio of the resistant moment to the driving moment:

$$\mathrm{FS} = \frac{\sum_{i=0}^{n} \tau_{fi} l_i}{\sum_{i=0}^{n} \tau_i l_i} \tag{1a}$$

$$\mathrm{FS} = \frac{\sum_{i=0}^{n} \tau_{fi} l_i r_i}{\sum_{i=0}^{n} \tau_i l_i r_i} \tag{1b}$$

where τ_i is the shear stress, τ_{fi} is the shear strength on the ith segment l_i along the failure surface, and r_i is the radius of the segment l_i with respect to the point where the moment is taken. The shear strength τ_{fi} can be expressed by the effective stress-based Mohr–Coulomb failure criterion:

$$\tau_{fi} = c_i + \sigma_i' \tan \phi' \tag{2}$$

where c_i is the cohesion on the ith segment of the failure surface, and σ_i' is the normal effective stress acting on the ith segment of the failure surface where the positive sign represents compression. For soil under saturated conditions, effective stress can be expressed by Terzaghi's effective stress principle, which is the difference between the total stress σ and pore water pressure u_w:

$$\sigma' = \sigma - u_\mathrm{w} \tag{3}$$

For soil under variably saturated conditions, Lu and Likos [17] unified effective stress principle by introducing the concept of suction stress σ^s:

$$\sigma' = \sigma - u_\mathrm{a} - \sigma^\mathrm{s} \tag{4}$$

where u_a is the pore air pressure and suction stress σ^s can be expressed as a function of matric suction $(u_\mathrm{a} - u_\mathrm{w})$ [16]:

$$\sigma^\mathrm{s} = -(u_\mathrm{a} - u_\mathrm{w}) \left\{ \frac{1}{1 + [\alpha(u_\mathrm{a} - u_\mathrm{w})]^n} \right\}^{1-1/n} \tag{5}$$

where α and n are the fitting parameters identical to van Genuchten's [24] soil water characteristic curve model that constitutively relates the volumetric water content θ to matric suction:

$$\frac{\theta - \theta_\mathrm{r}}{\theta_\mathrm{s} - \theta_\mathrm{r}} = \left\{ \frac{1}{1 + [\alpha(u_\mathrm{a} - u_\mathrm{w})]^n} \right\}^{1-1/n} \tag{6}$$

where the subscript r and s refer to the volumetric water content at the residual and saturated states, respectively.

The specific roles of all the previously mentioned mechanisms on the slope stability are generalized in the following conceptual model (Fig. 4a–e; Table 1). Figure 4a, b illustrates mechanical changes in Stage 1. Shortly after the impoundment of the reservoir, the increase in static load on the surface of the slope from the water-level rise produces three distinguishable mechanical mechanisms affecting the stability of the slope, as shown in the circles in Fig. 4b. The first mechanism is the shear component τ of the static water load on the slope surface that pushes upslope along the failure surface, resulting in a reduction in the driving shear force shown in the numerator of Eq. (1) (also see Fig. 4b), which leads to stabilization of the slope. The second mechanism is the increase in the total normal stress σ on the failure surface shown through Eqs. (1–3) (Fig. 4b), which leads to an increase in shear resistance and stabilization of the slope. The third mechanism is the potential fast seepage path through bedrock fractures, which could cause pore water pressure or suction stress to increase, resulting in a decrease in effective stress and shear strength shown in Eq. (1), and leading to destabilization of the slope. Thus, the net effect of all three mechanisms could either stabilize or destabilize the slope. However, as the time elapses (perhaps in late Stage 1 and early Stage 2), the reservoir water will seep into the slope and eventually reach the part of failure surface originally located above the water table, leading to three additional distinguishable mechanisms that affect the stability of the slope shown in the circles in Fig. 4c. The first mechanism is the increase in pore water pressure u_w below the water table and suction stress σ^s increase above the water table depicted in the middle circle, which results in a decrease in effective stress and factor of safety (Eqs. 1–5). The second and third mechanisms are due to the increase in the material's self-weight by wetting, which could lead to either stabilization or destabilization of the slope, depending on the angle of the failure surface and material's internal friction angle. The stabilizing effect (second mechanism) comes from the increase in the normal effective stress σ_i' and shear resistance τ_{fi} on the failure surface (see Fig. 4c; Eqs. 1–2), whereas the destabilizing effect (third mechanism) comes from the increase in the driving shear stress τ_i shown in Eq. (1) (also see Fig. 4c).

In Stage 3, during the annual fluctuation of the reservoir water level, the slope areas close to the reservoir are under cyclic wetting and drying conditions. When the reservoir water level is declining, reduction in the hydrostatic load on the surface of the slope would tend to increase the

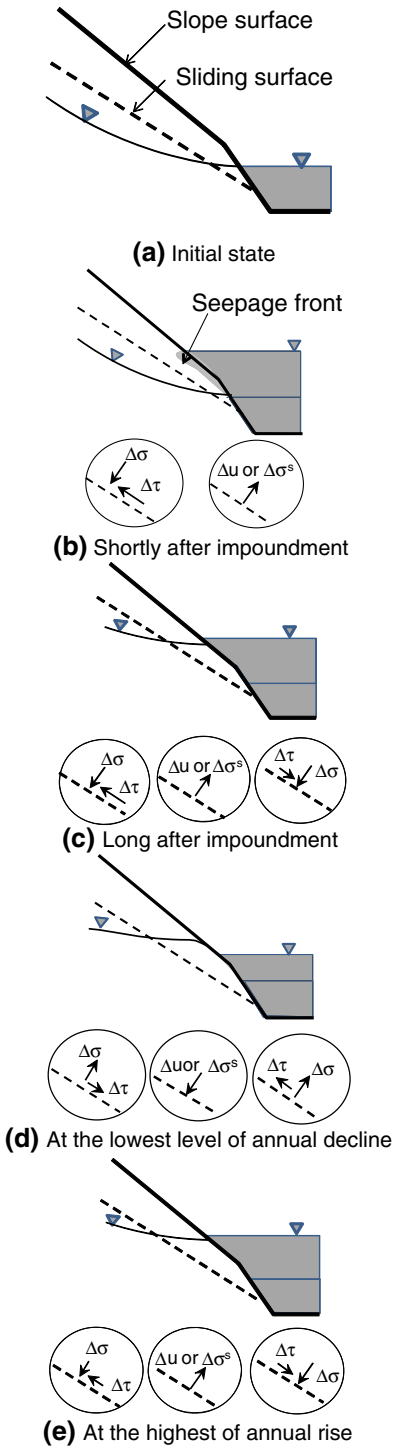

Fig. 4 Conceptual model of possible mechanisms for reservoir-induced landslides: **a** initial state, **b** shortly after impoundment, **c** long after impoundment, **d** at the lowest level of annual decline, and **e** at the highest level of annual rise

driving shear τ and decrease the shear strength term τ_{fi} by the reduction in total normal stress σ on the failure surface in Eq. (1) (depicted in the first circle in Fig. 4d), leading to destabilization of the slope. Depending on the slope's hydrologic conditions, the water table could decline too, leading to a decrease in pore water pressure u_w (below the water table) or suction stress σ^s (above the water table) (depicted in the middle circle in Fig. 4d), and leading to stabilization of the slope. Meanwhile, the self-weight of the slope could also be reduced during this stage, which could lead to either stabilization or destabilization of the slope (depicted in the third circle in Fig. 4d). Therefore, the net effect of reservoir operation to the stability of the slope is site specific, depending on the hydro-mechanical conditions of the slope and loading conditions. By the same token, in Stage 3 when the reservoir water level is rising, the opposite effects to that when the reservoir water level is declining could occur, as illustrated in Fig. 5e. Therefore, the net result to the stability of the slope is also site specific, depending on the hydro-mechanical conditions of the slope and loading conditions.

4 Field evidence of reservoir-induced landsliding

More than 30 boreholes have been drilled into the Huangtupo Slope to examine the subsurface hydrogeologic and geotechnical conditions. Six boreholes located in section A–A′, as shown in Fig. 2b, were advanced for sampling and subsurface mapping. These boreholes are (from north to south) HZK30, HZK5, HZK7, HZK8, HZK9, and HZK10. Before the impoundment of the reservoir, HZK5, HZK9, and HZK10 were dry, indicating groundwater level was below the bottom of these boreholes. But in HZK7 and HZK8, a perched water table was encountered at the elevations of 145.18 and 184.17 m, respectively. Therefore, the initial locations of the groundwater table at the Huangtpo slide No. 1 are below all of the above boreholes, and the perched water in HZK7 and HZK8 is caused by the low permeability of the local sliding zones.

The InSAR survey conducted at point P1 on Huangtupo Slope (see Fig. 2a for the location) and the results shown in Fig. 3b [18] clearly indicate that there is apparent correlation between the surface movement at P1 and the water-level fluctuations.

There are four locations where the surface displacement was monitored using GPS along the cross section A–A′ shown in Fig. 2b, namely G2, G7, G9, and G11 in the order from north to south. The GPS monitoring system is constructed by Trimble R7 Receiver and Trimble Zephyr Antenna with a plan accuracy of ± 5 mm + 0.5 ppm and a vertical accuracy of ± 5 mm + 1 ppm. The GPS data of the surface displacements for a 5-year period from April 2003 to March 2008 have been collected, and the results for the displacements as functions of time at these 4 locations are shown in Fig. 5a. The monitoring at G7, G9, and G11 started from April 2003, and G2 started from September

Table 1 Effects of different mechanisms on the stability of landslide as conceptualized in Fig. 4

Factors	Stage											
	Shortly after impoundment			Long after impoundment			At the lowest level of annual decline			At the highest of annual rise		
	Value	Effects	Slope stability	Value	Effects	Slope stability	Value	Effects	Slope stability	Value	Effects	Slope stability
Pore water pressure	↑	$\sigma\downarrow$	↓	↑	$\sigma\downarrow$	↓	↓	$\sigma\uparrow$	↑	↑	$\sigma\downarrow$	↓
Suction stress	↑	$\sigma\downarrow$	↓	↑	$\sigma\downarrow$	↓	↓	$\sigma\uparrow$	↑	↑	$\sigma\downarrow$	↓
Hydrostatic loading	↑	$\sigma\uparrow\&\tau\downarrow$	↑	↑	$\sigma\uparrow\&\tau\downarrow$	↑	↓	$\sigma\downarrow\&\tau\uparrow$	↓	↑	$\sigma\uparrow\&\tau\downarrow$	↑
Slope self-weight				↑	$\sigma\uparrow\&\tau\uparrow$	↓ or ↑	↓	$\sigma\downarrow\&\tau\downarrow$	↓ or ↑	↑	$\sigma\uparrow\&\tau\uparrow$	↓ or ↑

↑: value increase; ↓: value decrease; σ: normal stress; τ: driving shear stress

2004. These data represent the displacement history in the first three stages of the reservoir operation. In light of the proposed conceptual model, the characteristics of the displacements can be qualitatively explained as follows.

In the first 3 months of the initial reservoir impoundment from elevation 68 to 135 m (Stage 1), the increase in static load on the surface of the slope from the raised water level and the potential fast seepage through bedrock fractures control the stability of the slope. Thus, during this period, as conceptualized in Fig. 4a, b, the three mechanisms due to the increase in static load on the slope surface and the potential seepage counteract each other relative to the stability of the slide, resulting in little additional displacement of the slide. This is shown in the displacement data in Fig. 5a where small displacements were observed at G7, G9, and G11.

As the reservoir water level was maintained at the elevation of 135 m in the second stage from July 2003 to September 2006, inward and downward seepage into the slope occurred at rates governed by hydro-mechanical properties and the dimensions of the slope. When the water infiltrated through the main sliding zone, the water table further rose and the slope materials' self-weight increased. As identified in Fig. 4c, three mechanisms, namely stabilization by an increase in normal stress due to the weight increase, and destabilization by increases in pore water pressure and suction stress due to the water table rise and by an increase in driving shear stress due to the weight increase, will control the net effect on the stability of the slope. The displacement data collected during this stage shown in Fig. 5a indicate that the net effect was to destabilize the slope leading to continuous movement at all four locations. Two locations, G2-the closest to the reservoir and G11-the farthest to the reservoir, have relatively small displacement rates and total displacements (Fig. 5a, b, e), whereas the other two locations, G7 and G9, both are in the middle of the slope, experienced relatively large displacements rates and total displacements (Fig. 5a, c, d). Note that these two locations are above the thickest sliding zone (G7) and the steepest portion of the sliding surface (G9) (see Fig. 2b). These two facts tend to promote the mechanisms in destabilizing the slope and are possibly the reason for the large displacement rates and total displacements. The quantitative analysis of the net effect will be addressed in the later sections.

Another two observations on the displacement data at G7 and G9 shown in Fig. 5c, d can be made, the periodical variation in movement rate that is visually correlated with the reservoir water-level variations and the relatively steep rates of displacements in the first half of this stage from July 2003 to January 2005. The steep rates of the displacement could be coincident with the arrival of the wetting front at the sliding surface and wetting in the region beneath G7 to G9. During this period, pore water pressure or suction stress along the sliding surface or zone likely increased under variably saturated conditions, leading to significant decreases in effective stress and slope stability (FS). Under such scenario, the high rate of displacements experienced during the first half of the stage would not be sustained in the second half of the stage because the water table along the sliding surface would not propagate beyond the location beneath G9 or above the elevation 135 m (see Fig. 3). For G7 and G9 locations, it can also be observed during Stage 3 that the displacement rate (the slope of the displacement vs. time) is inversely correlated with the reservoir water-level rate, as shown in Fig. 5c, d. The quantitative analysis of these two observations will be conducted in the following sections.

5 Hydro-mechanical framework for variably saturated slopes

The traditional methods for slope stability analysis are mainly based on the concept of mechanical limit

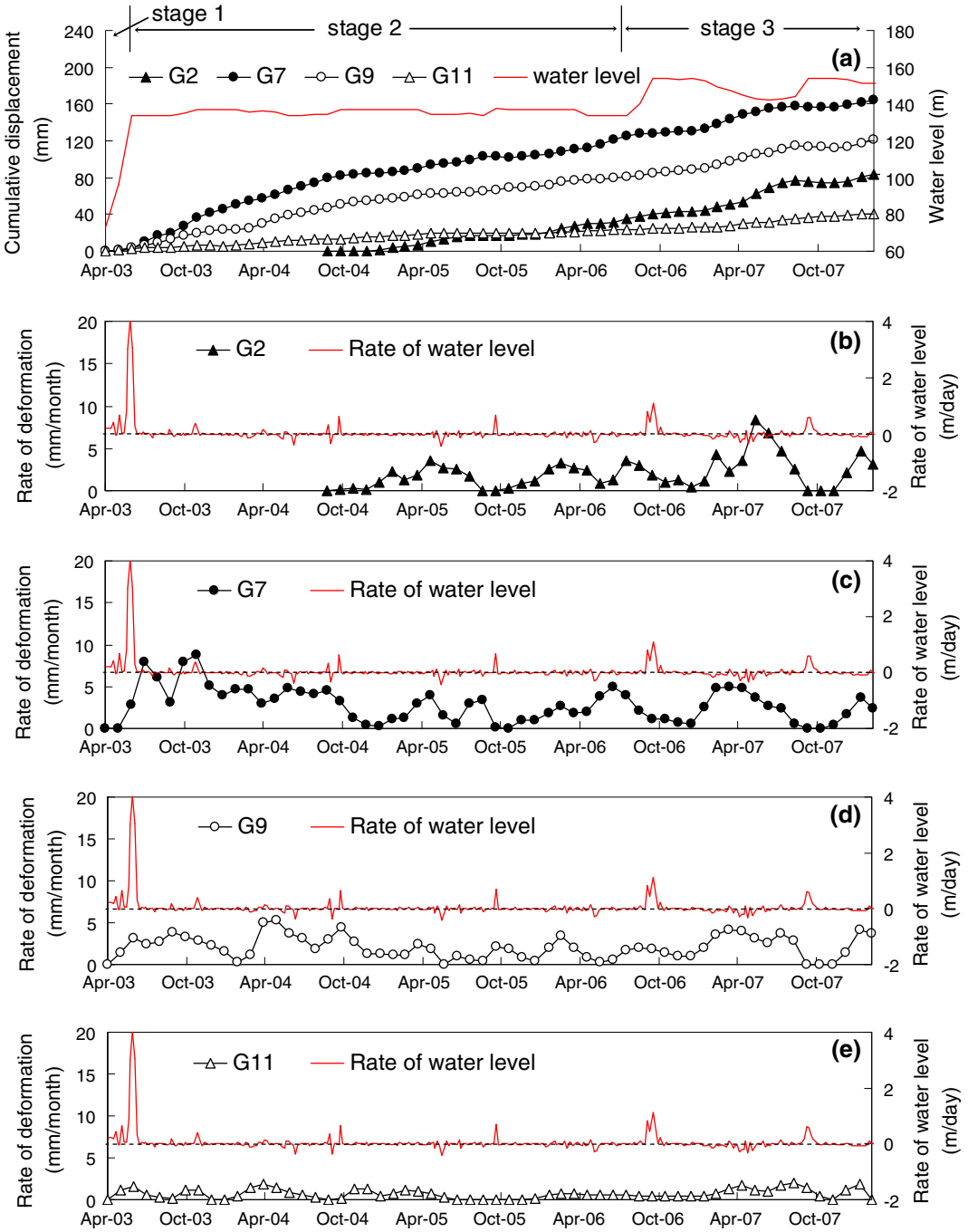

Fig. 5 GPS displacements at the locations shown in Fig. 2 from April 2003 to March 2008: **a** cumulative displacements, **b** rate of displacement at station G2, **c** rate of displacement at station G7, **d** rate of displacement at station G9, and **e** rate of displacement at station G11

equilibrium, which is used to analyze the stability of slopes by cutting the section of a slope into several vertical slices and calculate their force and moment equilibriums shown in Eq. (1) (e.g., [5]). With the widespread of availability of computer applications, numerical methods are commonly used in the calculation of slope stability (e.g., [3, 6, 19, 20, 28]). Hydro-mechanical frameworks have been used to evaluate the stability of variably saturated slopes by using effective stress principle (e.g., [1, 2, 7, 15]).

Mechanically and hydrologically, failure occurs when the state of effective stress reaches the shear strength of hillslope materials. When the water level in reservoirs rises, water seeps into hillslopes, causing the ground water table to increase in the region adjacent to reservoirs. Therefore, to evaluate the stability and predict the

occurrence of landslides in hillslopes adjacent to reservoirs, saturation and effective stress conditions within a hillslope should be analyzed and employed as a physical basis for slope stability assessments.

The detailed descriptions of the hydro-mechanical framework for variably saturated slopes can be found in Lu et al. [14] and Lu and Godt [15]. For completeness, a brief description is provided here. For quantifying transient water content field, Richards' equation [22] is employed:

$$\nabla \cdot K(h)\nabla H + W = \frac{\partial \theta(h)}{\partial t} \tag{7}$$

where $K(h)$ is the hydraulic conductivity function; h is the water pressure or suction head; H is the total water head equals to the sum of suction head and elevation; W is the inflow rate to receiving end or outflow rate from water source; and $\theta(h)$ is the volumetric water content that is a function of matric suction, as shown in Eq. (6).

The total stress in hillslopes mainly depends on the unit weight of slope materials and the additional stress caused by the hydrostatic pressure of the reservoir water on the slope surface. The total stress is governed by following linear momentum equilibrium equation.

$$\nabla \cdot (\boldsymbol{\sigma}) + \frac{\gamma}{g}\mathbf{b} = 0 \tag{8}$$

where $\boldsymbol{\sigma}$ is stress tensor with three independent total stress variables in the two-dimensional space; $\mathbf{b}$ is vector of body forces with two components; γ is the unit weight of materials and depends on water content; g is acceleration due to gravity.

After the total stress and pore water pressure have been computed by Eqs. (7) and (8), saturated zones and unsaturated zones can be divided by pore water pressure or saturation, and then, effective stress can be calculated by Eqs. (3–6). The factor of safety of each point of the landslide is calculated on the basis of above effective stress and shear strength parameters of landslide materials shown in Eqs. (1–2).

6 Two-dimensional model for the Huangtupo No. 1 slide

The two-dimensional numerical model shown in Fig. 6a was constructed from section A–A′ shown in Fig. 2b. Vertical and horizontal displacements were constrained on the bottom and both sides of the model, respectively. A varying head boundary condition controlled by the water-level record was applied on the right side of the model. A constant water head was applied at the left side assuming that it is sufficiently far from the reservoir and is thus not affected by the fluctuation of the reservoir water level. Because of the lack of sufficient hydrogeologic information for the deep bedrock, inverse modeling and the water table locations at the drilled boreholes were used to determine the seepage boundary conditions at the bottom and constant head on the left boundary. The optimum seepage velocity and constant water head are 1 m/day and 265 m, respectively. The upper stress boundary conditions consist of free stress and time-varying stress. The time-varying stress represents the hydrostatic force due to the fluctuations of the reservoir water level and was simulated in a simplified time-dependent function shown in Fig. 6b.

The hydro-mechanical properties are obtained from some previous work by Hubei Survey and Design Institute for Geo-hazard [9], and from the current investigation conducted at the Unsaturated Soil Mechanics Laboratory at Colorado School of Mines. These properties are listed in Table 2. The mechanical properties are bulk unity weight γ, Young's modulus E, Poisson's ratio μ, drained cohesion c', and internal friction angle ϕ'. The hydrologic properties are the parameters defining the soil water retention curve shown in Eq. (6), namely the inverse of air-entry pressure α, pore size distribution parameter n, residual water content θ_r and saturated water content θ_s, and the additional parameter defining the hydraulic conductivity function, namely the saturated hydraulic conductivity K_s. The hydraulic conductivity function is defined by Mualem's [21] model:

$$K = K_s \frac{\left\{1 - (\alpha|h|)^{n-1}\left[1 + (\alpha|h|)^n\right]^{\frac{1}{n}-1}\right\}^2}{\left\{1 + [\alpha|h|]^n\right\}^{\frac{1}{2}-\frac{1}{2n}}} \tag{9}$$

The numerical simulations are performed by using the commercial software package GeoStudio2007 (GeoSlope International, Ltd. 2007). Richards' equation (7) is solved using SEEP/W for fields of pressure head and water content, and total stress field (Eq. 8) is solved using SIGMA/W module and the SEEP/W module. SEEP/W does not consider the change in geometry with time. Slope stability is conducted with the SLOPE/W module, which employs the water content and pore pressure fields obtained from SEEP/W to assess contribution of pore water pressure or suction stress field (Eqs. 3–5) to shear strength, and the total stress field obtained from SIGMA/W was used to calculate factor of safety of the potential sliding surfaces. Because of the insufficiency in defining constitutive parameters pertaining to deformation properties of the slope material, linear elasticity model is used to calculate the deformation of the two-dimensional model. Therefore, the computed results of deformation have not been used to compare with the observed deformation data.

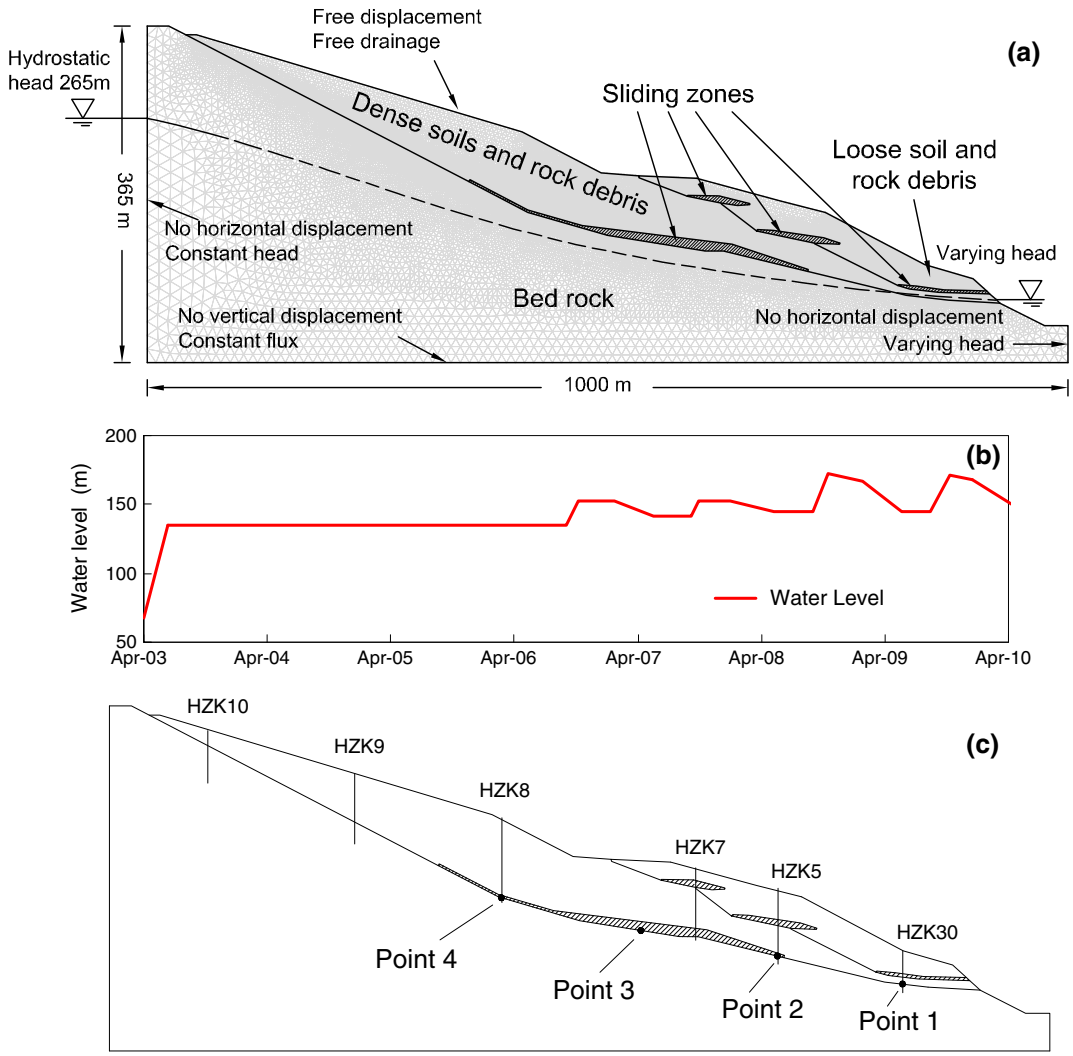

Fig. 6 A two-dimensional model for the No. 1 slide at the Huangtupo Slope: **a** FEM mesh and boundary conditions, **b** simulated water-level fluctuation from April 2003 to April 2010, and **c** vertical profiles at different locations for borehole sampling and modeling results

7 Modeling synthesis

The simulated pore water pressure distributions at different times under the initial reservoir impoundment and annual water-level fluctuation conditions are shown in Fig. 7. Before the impoundment of the Three Gorges Reservoir, the groundwater table is mainly below the interface of sliding zone and bedrock in the No. 1 slide, and only a small area of the toe is below the water table (Fig. 7a). The sliding zone above the water table is under unsaturated conditions and the pore water pressures are negative with values depending on elevation. After the impoundment of the Three Gorges Reservoir, significant changes in pore water pressure are observed in the sliding zone. The pore water pressure distributions for the times when the water level rose to elevations 135, 153, 175 m, and dropped to 145 m for the first time are shown in Fig. 7b–e. During Stage 1, the initial reservoir impoundment took place in less than 3 months from 68 to 135 m. Within this time frame, the pore water pressure changes were restrained in the toe area at the water table position but just advanced to the right tip of the thick sliding zone (see Fig. 7b in June 2003). This limited change in pore water pressure, together with the total stress increase, can be used to reconcile why only small displacements for the GPS locations shown in Fig. 5a were observed.

The pore water pressure increases continuously in Stage 2 when the water level remained at around 135 m for ~4 years and then rose quickly to 153 m in October 2006. By the end of Stage 2, the pore water pressure field has changed considerably in comparison with the initial conditions (see Fig. 7b, c). At this time, the water table has advanced to the middle of the sliding zones, and the negative pore water pressure there has increased from −750 to

Table 2 Hydrologic and mechanical properties of Huangtupo Slope

Material	γ (kN/m^3)	θ_s	c' (kPa)	ϕ' (°)	E (MPa)	μ	$1/\alpha$ (kPa)	n	θ_r	K_s (cm/s)
Bed rock	26.3[a]	0.1[a]	420.8[a]	44.5[a]	52,730[a]	0.23[a]	0.1[c]	7[c]	0.01[c]	1.16E−02[a]
Dense soil and rock debris	21.5[a]	0.4[a]	18.6[a]	18.3[a]	2,560[a]	0.28[a]	2.45[c]	2.8[c]	0.04[c]	8.10E−04[a]
Loose soil and rock debris	20.2[a]	0.42[a]	14.4[a]	16.8[a]	1,210[a]	0.31[a]	1.96[c]	2.6[c]	0.05[c]	2.20E−03[a]
Sliding zone soil	22.6[a]	0.32[a]	33.5[a]	10.6[a]	25.66[a]	0.34[a]	34.48[b]	1.24[b]	0.1[b]	6.59E−06[b]

[a] Provided in the survey report by Hubei Survey and Design Institute for Geo-hazard [9]

[b] Tested at Colorado School of Mines-US Geological Survey Geotechnical Laboratory

[c] Assumed values or values of similar materials from literature

−250 kPa, which indicates that the saturation of the whole sliding zone has increased. According to the suction stress-based unified effective stress principle, the negative pore water pressure increase from −750 to −250 kPa in sliding zone could cause about 200 kPa increase in suction stress or decrease in effective stress. This decrease in effective stress corresponds to the large displacements observed at the 4 GPS locations shown in Fig. 5a.

During Stage 3, from the end of September 2006 to the end of September 2008, the water level of the reservoir fluctuated annually between 153 and 145 m. The pore water pressure field continues to vary, and the water table has advanced above the entire sliding zone as shown in Fig. 7e. From October 2008 to April 2010 (Stage 4), the water level sharply rose and reached the highest design elevation of 175 m for the first time. After this period, it fluctuated annually between 145 and 175 m. From Fig. 7d, e, it can be seen that most of the sliding zone now is below the water table, and the region above the sliding zone is under cyclic drying and wetting conditions.

In order to compare the variation in stresses in different regions of the slide during the entire simulation period, four points of varying distance from the reservoir along the main sliding surface were selected (Fig. 6c). Point 1 is the closest to the reservoir beneath borehole HZK30 (Fig. 2b) and at the elevation of the initial reservoir water level. Point 2 is beneath borehole HZK5 and at the forefront of the thick sliding zone. Point 3 is at the middle of the sliding zone beneath G7. Point 4 is at the north end of the sliding zone beneath G9. The computed driving shear stress, resistant shear stress, total normal stress, effective normal stress, and pore water pressure at these four points along with the history of the water-level fluctuations are illustrated in Fig. 8. The simulation results quantitatively show that the variations in stresses in the Huangtupo Slope are greatly affected by the initial reservoir impoundment and the subsequent annual water-level fluctuations.

In Stage 1 of the initial reservoir impoundment when the water level rises from elevation 68 to 135 m, the total normal stress and pore water pressure at point 1 and point 2 increase, whereas they change slightly at point 3 and point 4, resulting in relatively large decreases in effective stress at point 1 and point 2 and small decreases in effective stress at point 3 and point 4 (Fig. 8). The relatively large decreases in effective stress at point 1 and point 2 are due to the proximity of these points to the reservoir where water seeps into this region as conceptualized in Fig. 4b. The reduction in effective stress leads to a reduction in shear resistance at these four points. The driving shear stress, on the other hand, remains relatively unchanged at all these points. The net effect, according to Eq. (1), is a decreasing trend in the factor of safety at these points shown in Fig. 9a.

In Stage 2 when the water level remained constant at 135 m for 4 years, all stresses remain relatively unchanged at point 1 and point 2, but not at point 3 and point 4 as water continues to seep into the slope. This is conceptualized in Fig. 4c. Specifically, total normal stress and pore water pressures at point 3 and point 4 continue to increase progressively, leading to decreasing trends in effective stress and shear resistance, as shown in Fig. 8c, d. As conceptualized in Fig. 4c, this is mainly due to the wetting along the sliding zone. This is well illustrated in the progressive pore water pressure increase at point 4 shown in Fig. 8d. The driving shear stress at these two points, on the other hand, remains relatively unchanged, indicating that the weight increase due to the wetting has a limited impact. The net effect is the decreasing trend in the local factor of safety shown in Fig. 9a.

During the 2-year period of Stage 3 when the water level varies annually between elevation 145 and 153 m, total normal stress and pore water pressure vary at a similar pace with the water-level fluctuation (Fig. 8a–d), but the effect diminishes at points further away from the reservoir. The resulting effective stress and shear resistance at these points, however, varies inversely proportionally to the water-level fluctuations, as it is best illustrated at point 3 shown in Fig. 8c. This is due to the time-delay effect in pore water pressure propagation. The change in the driving shear stress, mainly controlled by the weight of slope materials, is somewhat limited (Fig. 8a–d). The net effect on the stability, shown in Fig. 9a, is that for points (point 1 and point

2) close to the reservoir, the local factor of safety varies at a similar pace with the water-level fluctuation, but for points (point 3 and point 4) away from the reservoir, the local factor of safety varies in nearly the opposite manner. The time-delay phenomenon shown at points away from the reservoir is the result of transient water flow in the slide body.

The patterns of stresses in response to the 2-year annual water-level fluctuation in Stage 4, when the water level varies annually between elevations 145 and 175 m, are similar to that in Stage 3, except the magnitudes of the variation are larger, due to the higher annual water-level variation (30 m) (Fig. 8a–d). The reverse phenomenon of the effective stress shear resistance and the local factor of safety to the water-level variation pattern at point 3 and point 4 are more pronounced during this stage (Figs. 8c, d, 9a).

From the characteristics of the stress variations at the above four points during the water-level fluctuation, regions that experienced significant stress changes are consistent with the field GPS displacement observations. Following conclusions can be drawn: (1) effective stress is less affected by the fluctuation of water level in the toe region (point 1) and far from the reservoir (point 4), which is consistent with the small surface displacements observed at G2 and G11; (2) effective stress is greatly affected by the fluctuation of water level in the sliding zone (point 2 and point 3), which is consistent with the large surface displacements observed at G7 and G9; (3) the variation in the local factor of safety along the sliding surface exhibits the same periodic characteristics near the reservoir, but is reversed with respect to the fluctuation of the water level away from the reservoir.

According to the borehole survey data, there are four potential sliding surfaces within the No. 1 slide at the Huangtupo Slope (Fig. 9b). The main sliding surface is partially under the reservoir pool level, and the other three sliding surfaces are localized and secondary. The simulated factors of safety for all four potential sliding surfaces as functions of time are shown in Fig. 9c.

As shown in Fig. 9c, when the water level is at the initial elevation of 68 m, the factors of safety of all the potential sliding surfaces are greater than 1.0, indicating that the entire No. 1 slide is generally stable. Nevertheless, the factor of safety of the main (potential) sliding surface prior to the reservoir impoundment is only 1.03, indicating that it is vulnerable to failure. During Stages 1 and 2 when the water level quickly rose to 135 m and remained at that level for about 4 years, the factor of safety of the main potential sliding surface gradually decreased to 0.96 from the initial value 1.03. The factors of safety of Surfaces 2 and 3 slightly increased first when the water level reached 135 m and then gradually dropped to the values slightly less than the initial conditions during Stage 2. The factor of safety of Surface 4 decreases continuously.

Fig. 7 Modeling results of pore water pressure distributions during stages 1–3: **a** on April 15, 2003, when the water level is at its initial 68 m above the sea level, **b** on June 15, 2003, when the water level rose to 135 m in Stage 1, **c** on October 25, 2006, when the water level rose to 153 m for the first time, **d** on November 5, 2008, when the water level rose to 175 m for the first time, and **e** on June 19, 2009, when the water level declined to 145 m for the first time ▶

Because the factor of safety of the main potential sliding surface is always less than 1.0 in Stage 2, landslide motion was simulated, which is consistent with the observed surface deformation data shown in Fig. 5a. The displacements are generally continuous (Fig. 5a), and their rates vary from location to location (Fig. 5b–e). The highest displacement rate occurred at G7 monitoring points and is as much as 9 mm/month. After the water level of the Three Gorges Reservoir entered the annual fluctuation stages (Stages 3 and 4) in November 2006, the stability of the No. 1 slide increased slightly as the factors of safety for all 4 potential sliding surfaces increased with different amplitudes (Fig. 9c). The changes in the factor of safety for Surfaces 1 and 4 are relatively smaller, 0.04 and 0.07, respectively, whereas the factor of safety of Surfaces 2 and 3 increased 0.24 and 0.31, respectively. The increases in stability can be explained more by the increases in shear resistance rather than the driving stresses as illustrated in Fig. 8, indicating that the total normal stress change plays a dominate role in the stability of the Huangtupo Slide.

In the beginning of Stage 4 when the water level remained at 175 m for 4 months, the factor of safety of the potential sliding surfaces gradually decreased along all 4 potential sliding surfaces. When the water level fell back to 145 m, the factor of safety of all the potential sliding surfaces dropped to the lowest values. The factor of safety of the main sliding surface decreased to less than 1, but the other three potential sliding surfaces are always above 1.0, although they are lower than the initial values.

The cyclic variation in the factor of safety described above is consistent with the deformation data collected at the four GPS monitoring points and one InSAR monitoring point on the surface of the No. 1 slide shown in Figs. 3b and 5. Specifically, when the water level of the reservoir increased from the original elevation 68–135 m, the displacement of the surface accelerated. During the 4-year period when the water level remained around 135 m, the displacement rate accelerated in the first 2 years and then slightly decreased in the last 2 years. During the annual fluctuation periods, when the water level increased, the displacement rate at the monitoring points decreased. For example, the monitored displacements from August 2006 to February 2007 shown in Figs. 3b and 5a agree with the modeling result shown in Fig. 9c, indicating the suitability of the conceptual model illustrated in Fig. 4.

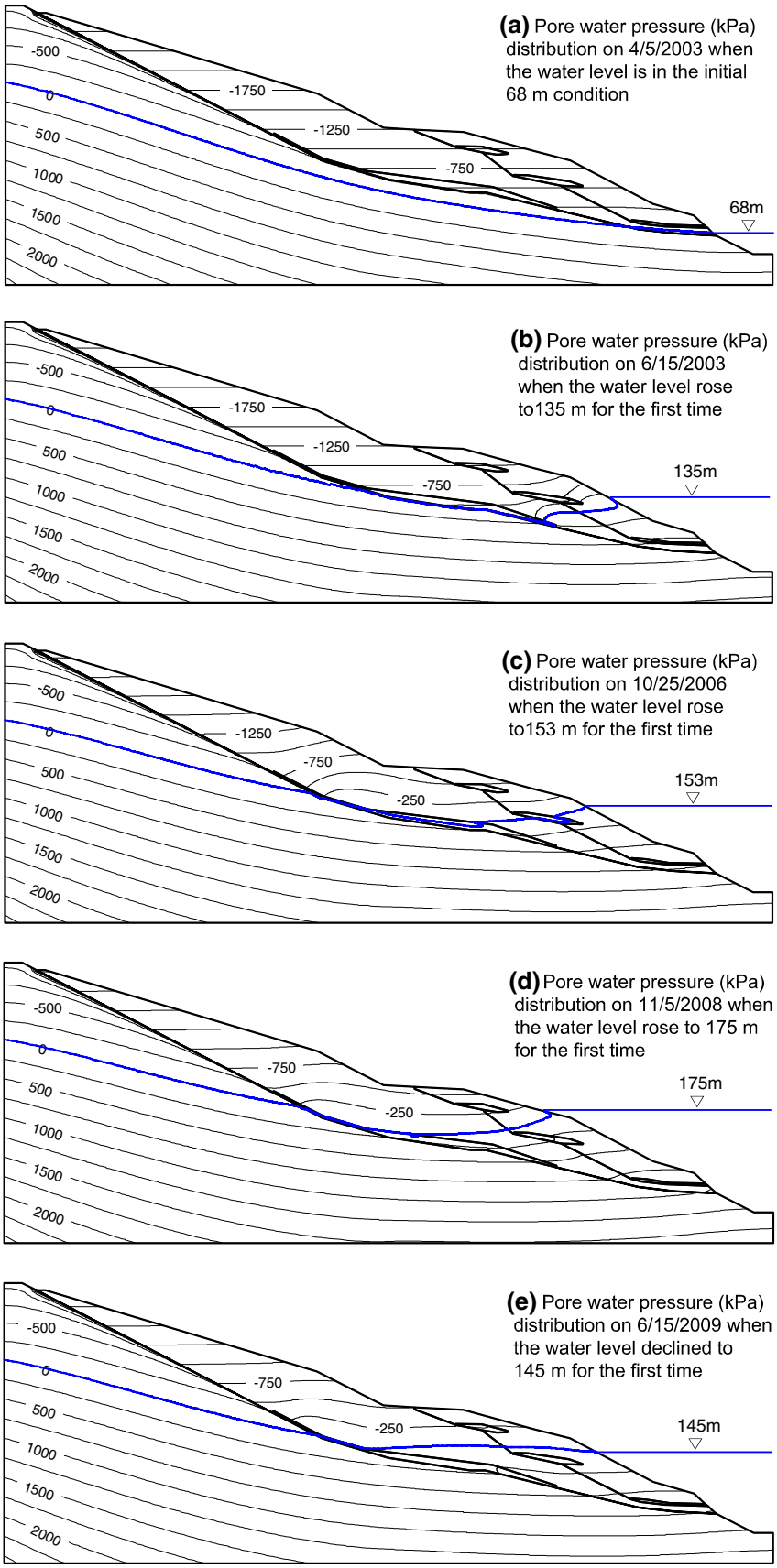

(a) Pore water pressure (kPa) distribution on 4/5/2003 when the water level is in the initial 68 m condition

(b) Pore water pressure (kPa) distribution on 6/15/2003 when the water level rose to135 m for the first time

(c) Pore water pressure (kPa) distribution on 10/25/2006 when the water level rose to153 m for the first time

(d) Pore water pressure (kPa) distribution on 11/5/2008 when the water level rose to 175 m for the first time

(e) Pore water pressure (kPa) distribution on 6/15/2009 when the water level declined to 145 m for the first time

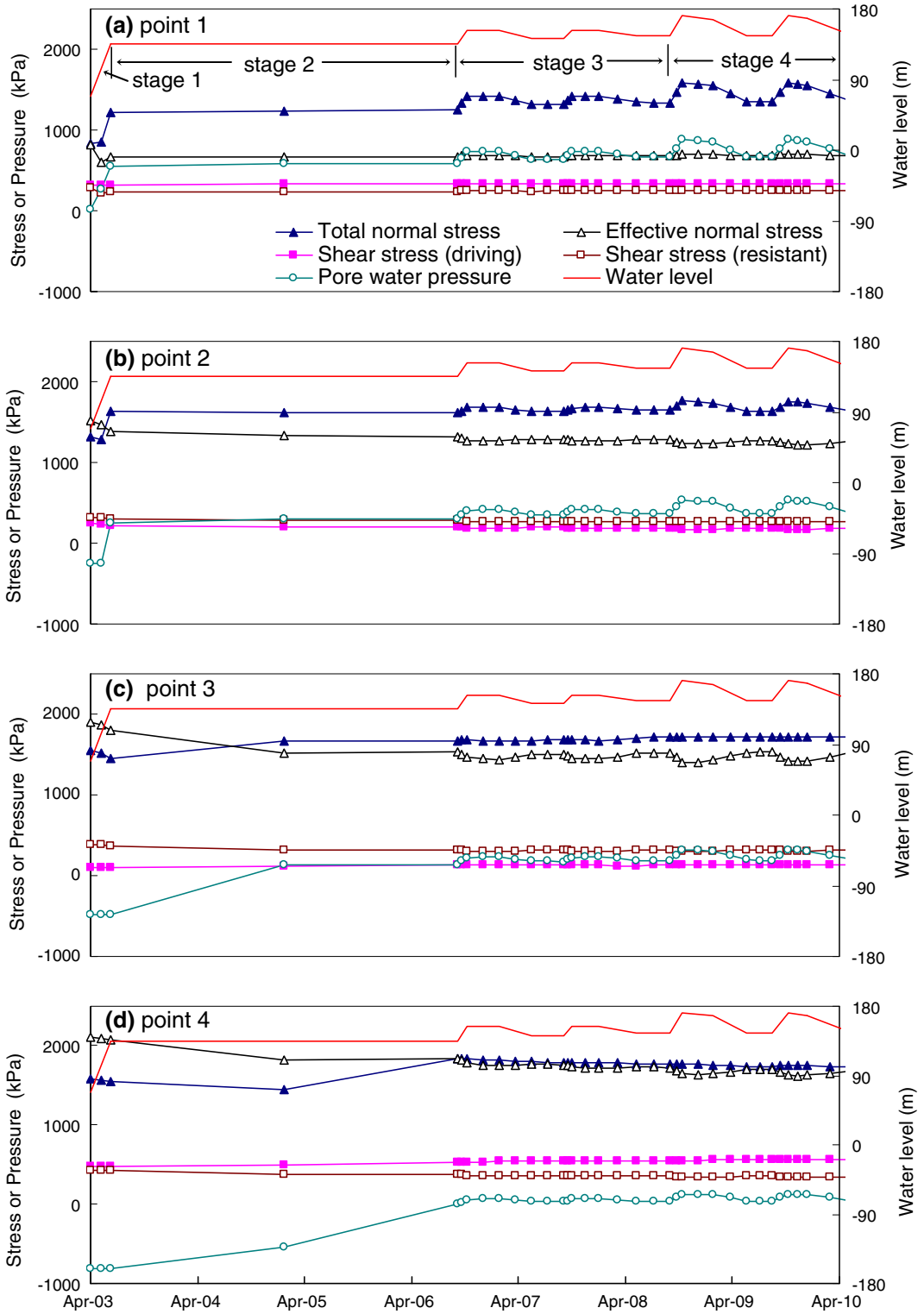

Fig. 8 Modeling results of different stress variations at the four different points along the main sliding surface within the No. 1 slide at the Huangtupo Slope: **a** point 1 at the toe region, **b** point 2 at the forefront of the sliding zone beneath borehole HZK5, **c** point 3 in the middle of the sliding zone beneath the surface GPS station G7, and **d** point 4 at the north end of the sliding zone beneath the surface GPS station G9

On the other hand, when the water level of the reservoir declined, the monitored displacement rate increased. For example, the monitored displacements from February 2007 to August 2007 shown in Figs. 3b and 5a agree with the modeling result shown in Fig. 9c, indicating the suitability of the conceptual model illustrated in Fig. 4.

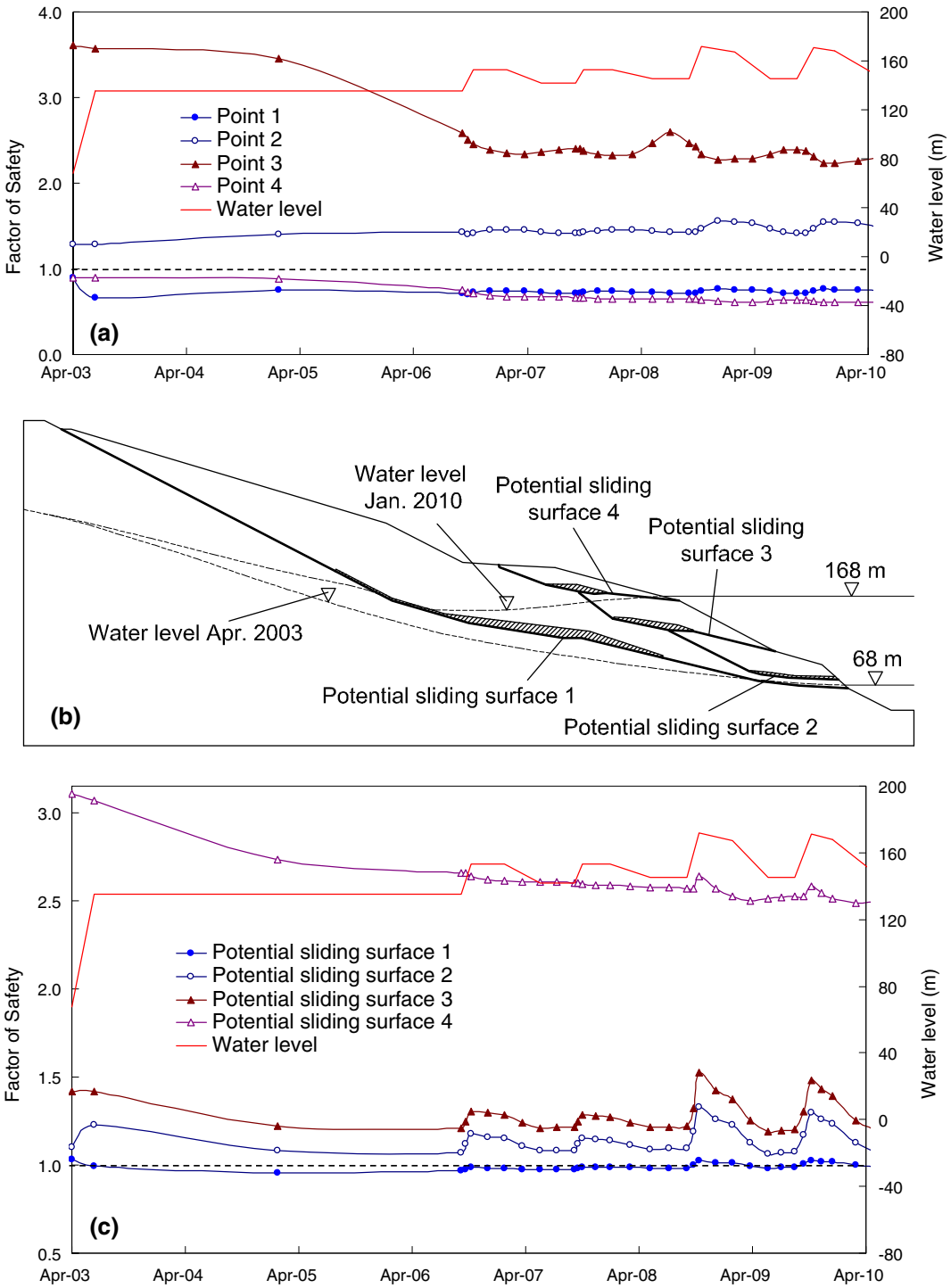

Fig. 9 Modeling results of variations of factor of safety within the No. 1 slide from April 2003 to April 2010: **a** at the four key points along the main sliding surface, **b** the locations of the potential four sliding surfaces, and **c** at the four potential sliding surfaces

8 Summary and conclusions

The Huangtupo Slope represents a typical persistently moving landslide in the Three Gorge Reservoir region. A multi-year monitoring program conducted on this slope indicates that there are multiple slides and the slope moves episodically toward the reservoir. Such movements of the slope appear to be highly correlated to the initial increase in the pool level of the reservoir and seasonal water-level changes. A general conceptual model is established for landslide movement triggered by initial reservoir impoundment and annual water-level fluctuations. Using

the conceptual model as a guideline, a two-dimensional hydro-mechanical numerical model is constructed to investigate quantitative link among the episodic movements and subsurface water content, suction, and effective stress variations from April 2003 to April 2010. Modeling results identify regions within the variably saturated slope where significant stress changes occur during the periods of the water-level rise from 68 to 175 m and of the seasonal fluctuation between 145 and 175 m. It is shown that the induced variations in pore water pressure, suction stress, hydrostatic loading, and slope self-weight have different effects on the effective stress conditions and slope stability. The field monitoring data and modeling synthesis also verify the general conceptual model.

The numerical model supports the proposed conceptual model for stabilizing and destabilizing mechanisms and the quantitative linkage between the observed episodic displacements and the water-level changes. Specifically, under the pre-impoundment conditions of 68 m water level, the factor of safety of the main sliding surface is slightly greater than 1.0, indicating that the Huangtupo Slope is stable, yet susceptible to landsliding. During Stage 1, the water level rose quickly to 135 m. The net effect of the hydrostatic load and the pore water pressure distribution is a decrease in the factor of safety. However, the slide experienced little displacement as the factor of safety is greater than 1.0. During Stage 2 when the water level remained around 135 m for 4 years, the factor of safety first gradually decreased continuously to about 0.96 in the first 2 years and then slowly increased to 0.97 at the end of the stage. This 2-step variation in the factor of safety can control the displacement rate and is confirmed by the field displacement data. In Stage 3 when the water level further increased to 153 m and fluctuated between 145 and 153 m from November 2006 to November 2008, the factor of safety is always less than 1.0 and varied with the annual water-level fluctuations. During this period, when the water level rose, the factor of safety increased. Conversely, when the water level decreased, the factor of safety decreased. This echoing behavior is also confirmed by the displacement data collected during this period and reconciled by proposed conceptual model. For Stage 4, when the water level further increased to 175 m and fluctuated between 145 and 175 m from September 2008 to September 2010, the factor of safety varies annually above and below 1.0, which approximately coincides with the water level increase (September to January) and decline (January to September) periods. Finally, this study suggests that the landslide movement will continue seasonally at the Huangtupo Slope under current reservoir operation, although it is challenging to predict whether there would be a catastrophic failure in the future.

Because the employed hydro-mechanical framework retains within the classical soil mechanics by extending effective stress principle under variably saturated conditions, a minimum modification to the classical slope stability analysis is needed. The modification involves using three constitutive relations of slope materials: soil water characteristic curve, hydraulic conductivity function, and suction stress characteristic curve. All of these three constitutive relations are defined by the common set of parameters. Thus, the shear strength criterion herein remains the same with the original Mohr–Coulomb expression, but the effective stress variation due to saturation variation is calculated by the unified effective stress expressed by Eqs. (4–5).

Acknowledgments This research is supported by the "Fundamental Research Funds for the Central Universities".

References

1. Borja RI, White JA (2010) Continuum deformation and stability analyses of a steep hillside slope under rainfall infiltration. Acta Geotech 5(1):1–14
2. Borja RI, Liu X, White JA (2012) Multiphysics hillslope processes triggering landslides. Acta Geotech 7(4):261–269
3. Dawson EM, Roth WH, Drescher A (1999) Slope stability analysis by strength reduction. Geotechnique 49(6):835–840
4. Deng QL, Zhu ZY, Cui ZQ, Wang XP (2000) Mass rock creep and landsliding on the Huangtupo Slope in the reservoir area of the Three Gorges Project, Yangtze River, China. Eng Geol 58(1):67–83
5. Duncan JM, Wright SG (2005) Soil strength and slope stability. Wiley, Hoboken
6. Griffiths DV, Lane PA (1999) Slope stability analysis by finite elements. Geotechnique 49(3):387–403
7. Griffiths DV, Lu N (2005) Unsaturated slope stability analysis with steady infiltration or evaporation using elasto-plastic finite elements. Int J Numer Anal Meth Geomech 29(3):249–267
8. Nakamra H, Wang G (1990) Discussions on reservoir landslide. Bull Soil Water Conserv 10(1):53–64
9. Hubei Survey and Design Institute for Geo-hazard (2001) Survey report of Huangtupo landslide in Three Gorges Reservoir area, BaDong, Hubei Province, China (in Chinese)
10. Jones FO, Embody DR, Peterson WL (1961) Landslides along the Columbia River Valley, Northeastern Washington. U. S. Geological Survey Professional Paper #367
11. Jian WX, Wang ZJ, Yin KL (2009) Mechanism of the Anlesi landslide in the Three Gorges Reservoir, China. Eng Geol 108(1–2):86–95
12. Li L (2002) Geological hazards and prevention in the Three Gorges dam area. Land Resour 4:4–7 (in Chinese)
13. Liao WL, Zhang LF, Yao YS (2009) Characteristics of seismicity in the Three Gorges Reservoir area. Seismol Geol 31(4):707–714
14. Lu N, Şener-Kaya B, Wayllace A, Godt JW (2012) Analysis of rainfall-induced slope instability using a field of local factor of safety. Water Resour Res 48(9). doi:10.1029/2012WR011830
15. Lu N, Godt JW (2013) Hillslope hydrology and stability. Cambridge University Press, Cambridge
16. Lu N, Godt JW, Wu DT (2010) A closed-form equation for effective stress in unsaturated soil. Water Resour Res 46(5). doi:10.1029/2009WR008646
17. Lu N, Likos WJ (2004) Unsaturated soil mechanics. Wiley, Hoboken

18. Liu P, Li ZH, Hoey T (2013) Using advanced InSAR time series techniques to monitor landslide movements in Badong of the Three Gorges region, China. Int J Appl Earth Obs Geoinf 21(4):253–264
19. Maiorano RMS, Russo G, Viggiani C (2013) A landslide in stiff, intact clay. Acta Geotech. doi:10.1007/s11440-013-0249-0
20. Meier J, Moser M, Datcheva M, Schanz T (2013) Numerical modeling and inverse parameter estimation of the large-scale mass movement Gradenbach in Carinthia (Austria). Acta Geotech 8(4):355–371
21. Mualem Y (1976) Hysteretical models for prediction of the hydraulic conductivity of unsaturated porous media. Water Resour Res 12(6):1248–1254
22. Richards LA (1931) Capillary conduction of liquids through porous medium. J Phys 1(5):318–333
23. Sun K, Li K, Sun ZY (2011) The environmental assessment of the sediment after preliminary impounding of Three Gorges Reservoir. Energy Procedia 5:377–381
24. van Genuchten MT (1980) A closed-form equation for predicting the hydraulic conductivity of unsaturated soils. J Soil Sci Soc Am 44(5):892–898
25. Wang Y, Yin KL (2004) Perturbation method of superposing initial surge height of landslide along reservoir shoreline. Chin J Rock Mech Eng 23(5):717–720 (in Chinese)
26. Wen BP, Chen HY (2007) Mineral compositions and elements concentrations as indicators for the role of groundwater in the development of landslide slip zones: a case study of large-scale landslides in the Three Gorges Area in China. Earth Sci Front 14(6):98–106
27. Wen BP, Aydin A, Aydin NS, Li RR, Chen HY, Xiao SD (2007) Residual strength of slip zones of large landslides in the Three Gorges area, China. Eng Geol 93(3–4):82–98
28. Xu T, Xu Q, Tang CA, Ranjith PG (2013) The evolution of rock failure with discontinuities due to shear creep. Acta Geotech 8(6):567–581
29. Zhao J, Fu G, Lei K, Li YW (2011) Multivariate analysis of surface water quality in the Three Gorges area of China and implications for water management. J Environ Sci 23(9):1460–1471